Homolytic Products from Heterolytic Paths in H_2 Dissociation on Metal Oxides: The example of CeO_2

Journal:	*The Journal of Physical Chemistry*
Manuscript ID:	jp-2014-02309r.R1
Manuscript Type:	Article
Date Submitted by the Author:	n/a
Complete List of Authors:	García-Melchor, Max; Institute of Chemical Research of Catalonia (ICIQ), Lopez, Nuria; Institute of Chemical Research of Catalonia (ICIQ),

Homolytic Products from Heterolytic Paths in H_2 Dissociation on Metal Oxides: The example of CeO_2

Max García-Melchor and Núria López**

Institute of Chemical Research of Catalonia (ICIQ), Av. Països Catalans, 16, E-43007 Tarragona, Spain.

Keywords: density functional theory, metal oxides, ceria, H_2 dissociation, homolytic, heterolytic,

Abstract

Mechanisms for H_2 dissociation on metal oxides have been typically inferred from the infrared spectra of reaction products on the basis of the presence or lack of M–H fingerprints. Here, we demonstrate by means of Density Functional Theory that oxides with polar M–O bonds favor heterolytic dissociation. Moreover, we report that the resulting heterolytic product can further evolve to the homolytic one provided that metal ions are reducible. Hence, it follows that the redox capacity of the metal determines the reaction outcome. This finding sheds light on why both M–H and O–H bands appear in the infrared spectra of non-reducible oxides such as MgO or γ-Al_2O_3, while only O–H bands are observed for reducible oxides like CeO_2. It results in a unified mechanism for polar oxides that can be generalized to other materials exhibiting significant charge separation. Importantly, we also show that the low activity of CeO_2 towards

H_2 can be improved by enhancing the basicity of surface O atoms upon lattice expansion. This may pave the way for the efficient use of CeO_2 in selective hydrogenation reactions and for the further advance on processes involving dissociation of non-polar bonds like C–H.

1. Introduction

Molecular hydrogen dissociates through one of the mutually exclusive homolytic or heterolytic pathways. On metal oxides, MO_x,[1,2] homolytic (radicalary) dissociation produces two hydrogen atoms that combine with two oxygen sites leading to the formation of two O–H groups, with the concomitant reduction of two surface metal ions (Eq. 1). Alternatively, heterolytic (polar) dissociation entails the formation of a hydride, H^-, and a proton, H^+, which adsorb on metal and oxygen centers yielding M–H and O–H species, respectively (Eq. 2).

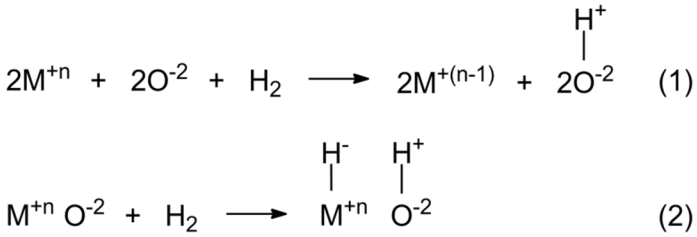

$$2M^{+n} + 2O^{-2} + H_2 \longrightarrow 2M^{+(n-1)} + 2\,(H^+ \,|\, O^{-2}) \quad (1)$$

$$M^{+n}\,O^{-2} + H_2 \longrightarrow (H^- \,|\, M^{+n})\,(H^+ \,|\, O^{-2}) \quad (2)$$

So far, the mechanistic proposal for dissociative H_2 adsorption on MO_x has been based on the existence in the infrared spectra of either both O–H and M–H bands for the heterolytic pathway, or only O–H bands for the homolytic path.[3-8] Hence, heterolytic cleavage has been assumed to occur on non-reducible oxides such as MgO or γ-Al_2O_3,[3-5] whereas homolytic cleavage has been assumed for reducible oxides such as TiO_2 or CeO_2.[6-8]

Herein, we provide firm theoretical evidence that the above *a priori* excluding mechanisms can be interconnected. More specifically, we report that heterolytic dissociation of H_2 can also afford the homolytic product, and that the preference for one pathway or the other, as well as the reaction outcome, depends on the physicochemical properties of the given MO_x. Therefore,

experimental evidences for the products do not ensure that the activation mechanism can be successfully traced back.

For the present study, we chose ceria, CeO_2, as a representative reducible MO_x (Figure 1). Ceria participates in a number of industrially attractive applications involving H_2 formation or dissociation such as ethanol steam reforming,[9-10] the water-gas shift reaction,[11-12] and the selective hydrogenation of alkynes.[13-14] Furthermore, CeO_2 has a prominent role in several oxidation processes like three-way automotive-exhaust catalysis,[15] solid oxide fuel cells,[16-17] or HCl oxidation.[18-19] These applications depend in turn on the oxygen storage capacity, which is directly linked to the presence of oxygen vacancies that can be created by reduction with H_2.[20]

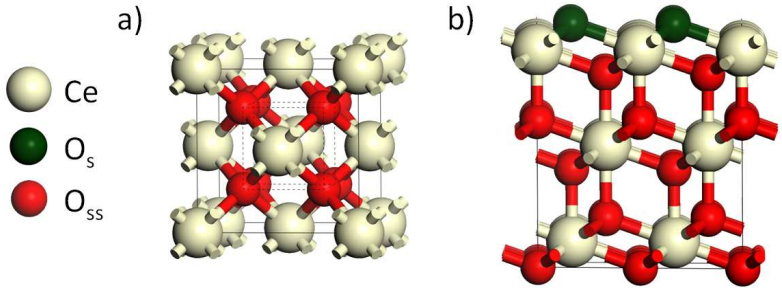

Figure 1. Representation of (a) the CeO_2 lattice and (b) a CeO_2(111) surface.

H_2 adsorption on CeO_2 has been extensively investigated by means of different experimental techniques including Temperature-Programmed Reduction (TPR) and Fourier-Transform Infrared (FTIR) spectroscopy.[6,21-23] The TPR measurements[21-23] typically show two peaks around 750 and 1000 K, which are attributed to surface and bulk reduction, respectively. The stretching bands appearing in the 3500-3700 cm^{-1} region of the FTIR spectra[6,21] are assigned to free hydroxyl groups with different coordination and to bound water molecules, while no Ce–H bands have been assigned in the region where they should appear (*ca.*1500 cm^{-1}).[24]

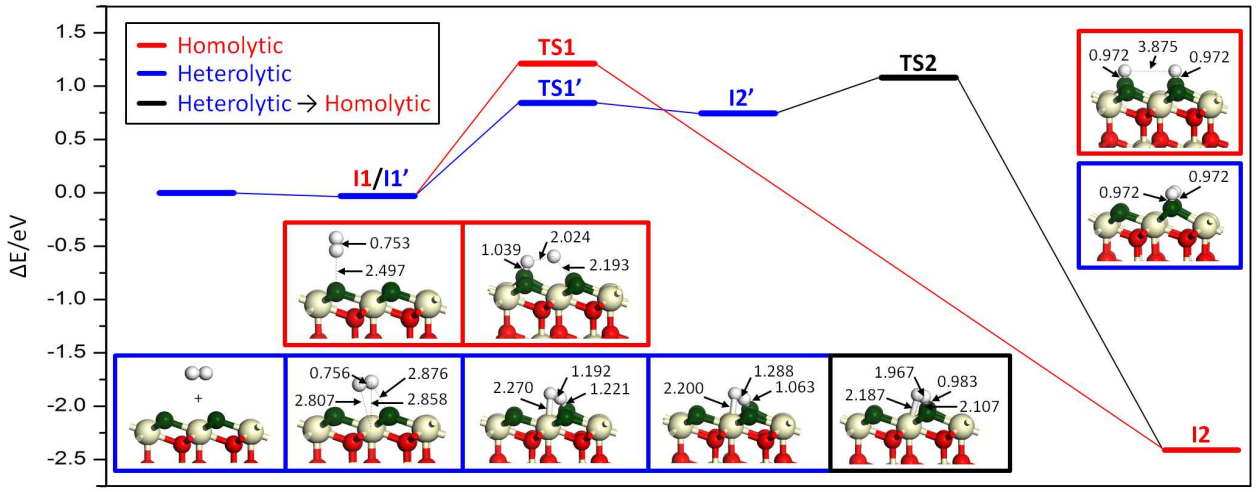

Figure 2. Energy profiles for the homolytic (in red) and heterolytic (in blue) reaction pathways in the H_2 dissociation on CeO_2(111). The transition state linking the heterolytic and homolytic products is shown in black. Optimized geometries with relevant bond distances (Å) are also shown.

On the basis of the FTIR data, and as with all reducible oxides,[6-8] a homolytic pathway has been presumed for H_2 dissociation on CeO_2.[7,13-14,25-29] This mechanistic proposal is, however, indirect as none of the above experimental observations can provide conclusive evidences of the operating mechanism. While the use of computational methods might greatly contribute to shed light on this issue, all the theoretical works reported to date[7,14,25-29] have only considered a homolytic path, neglecting heterolytic activation. Hence, the aim of the present work is to compare and evaluate the homolytic and heterolytic paths for H_2 activation on CeO_2 and use this knowledge to set the basis for predicting the reactivity of H_2 on any MO_x.

2. Theoretical methods

All the DFT calculations presented in this work were performed using the Vienna ab initio simulation package (VASP, version 5.3.2).[30,31] The valence electrons Ce ($5s^2 5p^6 4f^1 5d^1 6s^2$) and O ($2s^2 2p^4$) were expanded in plane waves with a cutoff energy of 500 eV, while the core electrons were represented by projector-augmented wave (PAW) potentials.[32] Given the strongly correlated nature of CeO_2, the Perdew-Burke-Ernzenhof (PBE) generalized-gradient approximation functional[33] was employed and the self-interaction error was mitigated through the addition of a *U* Hubbard-like term. This was carried out following the approach of Dudarev *et al.*,[34] which defines the difference between the Coulomb, *U,* and exchange, *J,* parameters as the effective *U* parameter, U_{eff}. For Ce atoms, a value of U_{eff} = 4.5 eV was chosen on the basis of the satisfactory results reported in previous theoretical works.[35-37]

Ceria is a semiconductor adopting a fluorite structure (*Fm3m*, Figure 1a) with an experimentally determined lattice constant of a_{exp} = 5.411 Å.[38] The lattice constant calculated in this work using a dense Γ-centered 7×7×7 k-point mesh was a_{calc} = 5.497 Å, which is in good agreement with the experimental value and previous theoretical studies.[36,39] To simulate the CeO_2(111) surfaces, periodically repeated slabs of three O−Ce−O trilayers with a vacuum space of at least 14 Å between them were constructed (Figure 1b). The geometry of these surfaces with a *p*(2×2) periodicity was optimized using a Γ-centered 3×3×1 mesh for the k-point sampling. During optimizations, the five outermost layers were allowed to relax, whereas the four bottom layers were kept fixed to their bulk positions. Total energies were converged better than 10^{-5} eV in the self-consistent field and geometries were relaxed until the energy convergence criterion of 10^{-4} eV was fulfilled. Spin polarized calculations were carried out when needed, and a careful analysis of the localization of the excess of charge was performed (Tables S1 and S2). The

reported Bader charges were calculated using the charge densities obtained with VASP and the program developed by Henkelman *et al*.[40-42]

For the location of transition states, the Climbing Image Nudged Elastic Band (CI-NEB) algorithm[43] was employed using at least five images along the reaction coordinate. The geometries for these saddle points were optimized with the same energy threshold used for the optimization of the reaction minima. The nature of the transition states, as well as the minima connecting these saddle points, was assessed by performing numerical frequency analysis.

The above PBE+*U* methodology was compared with benchmark calculations using the HSE06 hybrid functional developed by Heyd−Scuseria−Ernzerhof,[44] see Table S1. As hybrid functionals are computationally much more demanding than DFT+*U*, calculations with the HSE06 functional were carried out with a reduced cutoff energy of 400 eV and with a Γ−point sampling. The resulting energies with this hybrid functional are very similar to those obtained with PBE+*U*, which supports the good performance of the latter methodology.[20]

3. Results and discussion

We first investigated the homolytic and heterolytic pathways for H_2 dissociation on the most exposed CeO_2(111) surface. The energy profiles obtained for these two paths are shown in Figure 2. In both mechanisms, the initial interaction between H_2 and the regular ceria surface (**I1/I1'**) was found to be thermoneutral, with only slightly elongated H–H bond distances (less than 1 %). In the case of the homolytic precursor (**I1**), the H_2–surface interaction concerns only one of the two hydrogen atoms and a surface O atom, whereas in the heterolytic precursor (**I1'**) both hydrogens interact with the surface through Ce and O centers.

Once **I1** is formed, the subsequent homolytic cleavage takes place on two contiguous surface oxygens, which gives rise to the formation of two O–H groups (**I2**). This dissociation is highly

exothermic (by *ca.* 2.4 eV) and causes the change in the oxidation state of two cerium cations from Ce^{+4} to Ce^{+3}.[45] The transition state located for this step (**TS1**) displays a highly stretched H–H distance of 2.024 Å, and has a relatively high energy barrier of 1.21 eV.[46]

On the other hand, the heterolytic dissociation from **I1'** occurs on adjacent Ce and O sites, which leads to the formation of the corresponding Ce–H and O–H bonds (**I2'**). Unlike the homolytic pathway, this step is endothermic by 0.75 eV and exhibits a much smaller energy barrier of 0.85 eV (**TS1'**). Interestingly, the H Bader charges in **I2'**, ±0.45 |e-|, show a strong polarization of the H–H bond. Moreover, the H–H distance is relatively short, 1.288 Å, which suggests an electrostatic interaction between the generated hydride (Ce–H) and the proton (O–H). Indeed, the analysis of the charge density difference (Figure 3a) confirmed that **I2'** is better described as a tight ion-pair.[47] Similar structures to **I2'** have been also recently reported for MgO and γ-Al_2O_3.[4,48]

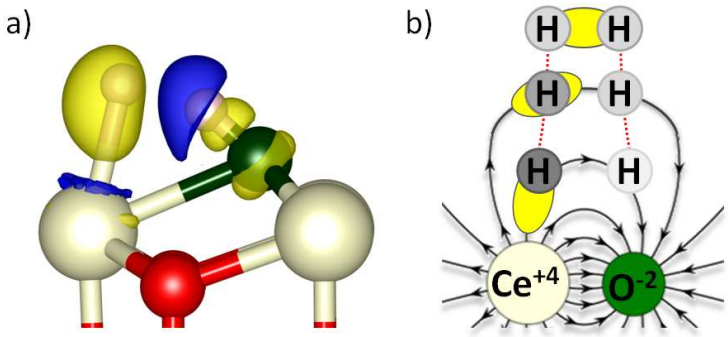

Figure 3. (a) Charge density difference in **I2'** illustrating the formation of the H^+–H^- tight ion-pair. Yellow (blue) zones indicate electron density accumulation (depletion). The isocontour corresponds to 0.010 $Å^{-3}$. (b) Schematic representation of the polarization of the H_2 σ-bonding orbital caused by the surface electric field in the heterolytic path. The increase (decrease) of the grey intensity for H accounts for the charge accumulation (depletion).

Overall, according to the energy profiles depicted in Figure 2, the homolytic dissociation is thermodynamically favored, whereas the heterolytic one is kinetically most likely. Even so, the metastability of the heterolytic product, **I2'**, implies that the population of the ion pair under normal conditions is rather small. Thus, unless **I2'** evolves into a more stable species, the homolytic pathway shall be the long-run operating mechanism. One possibility to enable the heterolytic path would be that **I2'** could develop into the homolytic product, **I2**. Should this happen, then the heterolytic and homolytic paths would be linked. This **I2'** to **I2** interconversion would entail breaking the tight ion pair and transferring the H atom from the Ce–H moiety to a neighboring surface oxygen, with the concomitant reduction of two Ce cations. The transition state (**TS2**) associated to this step is 0.13 eV lower in energy than that for the homolytic dissociation (**TS1**). Therefore, H_2 does not dissociate homolytically on CeO_2(111), but via a heterolytic pathway (**TS1'**) followed by the transfer of a hydrogen atom (**TS2**) that finally yields the homolytic product (**I2**).

Having established the reaction mechanism for H_2 dissociation on CeO_2, we next aimed at generalizing these results to predict the reactivity of H_2 on any MO_x. For this purpose, the following considerations need to be taken into account. The homolytic and heterolytic bond dissociation energies (BDE) for H_2 are 4.52 and 17.36 eV, respectively.[49] Thus, homolytic dissociation prevails over the heterolytic one unless this energy difference is offset. This is the case of CeO_2, on which the heterolytic BDE for H_2 is reduced to the point that this dissociation is preferred over the homolytic one.

The energy compensation in favor of the heterolytic path stems from the nature of the H_2–CeO_2 interaction. That is, the oppositely charged Ce and O surface ions, with Bader charges +2.33 and -1.20 |e-|, respectively, generate a strong electric field on the outer surface that

polarizes the H_2 molecule as it approaches the surface (Figure 3b). The polarization of the H–H bond results in the stabilization of **I2'** thus favoring the heterolytic dissociative adsorption. This was confirmed by calculating the electrostatic contribution to the energy of **I2'**, $E_{Coulomb}$, as: $E_{Coulomb} = E_{H+} + E_{H-} + E_{H+–H-}$, where the terms E_{H+} and E_{H-} stand for the electrostatic energy of the proton and the hydride, respectively, in the on-site Madelung potential generated by the oxide, and $E_{H+–H-}$ is the electrostatic interaction in the tight ion-pair, see Supporting Information. The estimate $E_{Coulomb}$, taking into account the interatomic distances and Bader charges in **I2'**, is -16.4 eV. This energy lowers the heterolytic BDE for H_2 to 0.96 eV, which nicely agrees with the calculated value for **I2'** shown in Figure 2. The stabilization of this dissociative adsorption has been also qualitatively proposed by Metiu *et al.*[50] in terms of formation of an acid-base pair on the surface.

The above analysis can be extrapolated to any MO_x or even other classes of materials. In this way, a qualitative analysis considering typical M–H and O–H distances, *i.e.* 2.200 Å and 1.100 Å, respectively, points out that the charge separation in a MO_x shall be larger than 1 |e-| in order to make the heterolytic pathway accessible. Therefore, for MO_x with such polarized M–O bonds, heterolytic dissociation will predominate as only electrostatic contributions are enough to compensate the energy penalty associated with this process. This explains the high energy barrier reported on SiO_2 (2.05 eV),[51] as Si–O bonds are not sufficiently polarized to activate H_2. Moreover, it suggests that for other high symmetry molecules with a relatively inert bond such as C–H, *e.g.* CH_4, the same considerations may apply.

Importantly, when heterolytic dissociation is preferred, the energy of **TS2** (Figure 2) is crucial for predicting the outcome of the reaction, since it connects the heterolytic and homolytic products. This transition state involves the reduction of two metal ions and, accordingly, it

essentially depends on the ease in the electron exchange between the $M^{+n}/M^{+(n-1)}$ redox pair. Therefore, the higher the reduction potential of the cation is the lower the energy penalty for **TS2** will be. That is to say, this reaction channel linking the heterolytic and homolytic pathways is only accessible for reducible oxides. Proof of it is that only the heterolytic product is obtained in H_2 dissociation on non-reducible oxides like MgO or γ-Al_2O_3.[3,5]

Still, H_2 activation by CeO_2 is poor since it is hindered by a relatively high energy barrier. This is in agreement with recent experimental works on selective hydrogenation reactions, where a high H_2/hydrocarbon ratio or the use of a more reducing agent like N_2H_4, have been reported to be necessary to reach significant activity.[13-14,52] Given the need for a solution and the reported effect of strain in oxide surfaces,[53,54] we focused on trying to improve H_2 dissociation on CeO_2 by applying geometric distortions to the lattice. Ceria forms solid solutions with many lanthanides resulting in an almost continuous tuning of the lattice parameters.[55] Hence, we investigated the above homolytic and heterolytic pathways on several strained CeO_2(111) surfaces in order to simulate the geometric distortions that can be easily induced by doping (±5%).

Similarly to the unstrained surface, heterolytic dissociation dominates in all the investigated cases, though depending on the type of strain, the energetics of the two paths are affected in a different way. In particular, lattice expansion lowers both energy barriers for H_2 dissociation, while the contrary happens for compressive strains. Then H_2 activation rate is improved by 4 orders of magnitude upon strain at typical hydrogenation temperatures (T = 373 K). To get a deeper insight into the origin of these trends, we calculated the center (weighted average) of the O(2p) band in the PDOS of the different strained surfaces, which has been reported to be a good descriptor for the Lewis basicity of O atoms.[48] The H_2 activation energies as a function of the

center of the O(2p) band are presented in Figure 4. Interestingly, for both dissociative processes a linear relationship between the activation energy and oxygen basicity exists. The reason behind the enhanced activity is that lattice expansion shifts the O(2p) band closer to the Fermi level, which improves the basicity of O atoms making them more prone to accept the protons derived from H_2 activation. Moreover, it should be noted that the slope of the line for the homolytic pathway is considerably higher than that for the heterolytic one, which underlines the stronger dependency of this mechanism on the basicity of O atoms. This is perfectly consistent with the geometries and slopes for the two dissociative trajectories (Figures 2 and 4) as two oxygen atoms are involved in the homolytic dissociation, while only one in the heterolytic process.

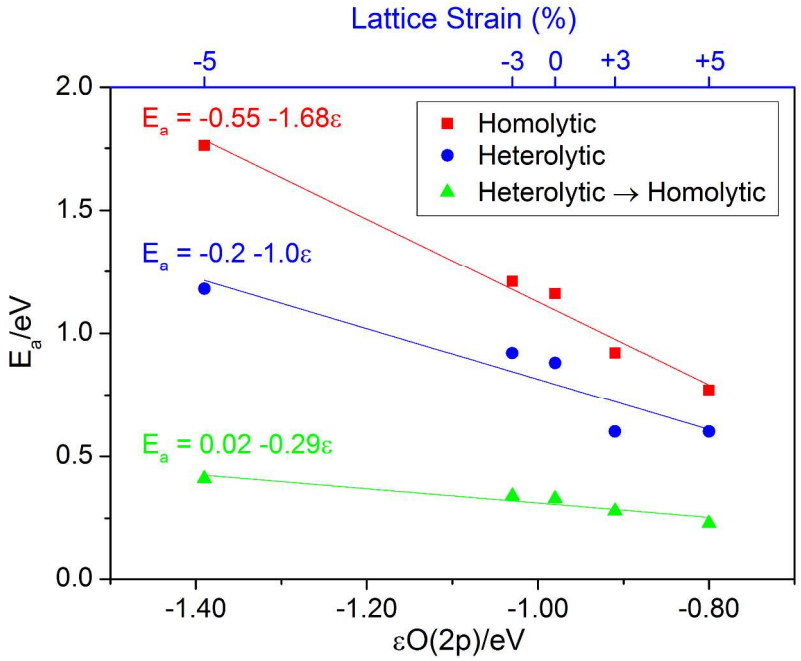

Figure 4. Activation energy, E_a, for the H_2 dissociation on strained $CeO_2(111)$ surfaces as a function of the center of the O(2p) band, εO(2p), and the corresponding Lattice Strain (top x-axis). Equations for the linear fittings are presented here, while the corresponding statistics are shown in Table S3.

In contrast, Figure 4 clearly shows that the reaction pathway linking the heterolytic and homolytic mechanisms (**TS2**) is hardly affected by lattice strain, confirming the local nature of this elementary step associated to the metal redox properties. The electronic effects induced by the addition of dopant cations might also have a direct effect on the reaction barriers, and thus, they should also be considered for further improvements.

4. Conclusions

In summary, our analysis points out that dissociative H_2 adsorption on CeO_2 takes place through a heterolytic pathway followed by the transfer of a H atom that finally yields the homolytic product. This mechanism accounts for the reported final product, but it is conceptually different from the so far presumed homolytic pathway. Hence, this finding warns that experimental evidences of the reaction products might be deceptive for the assignment of the operating mechanism. Besides, we provide the basis for predicting the outcome of H_2 dissociation on any MO_x, showing that both the polarization of the M–O bond and the redox capacity of the metal ions are decisive to understand the activation mechanism and the nature of the products. We also report that this reaction can be tuned upon lattice strain. In particular, we predict that lattice expansion improves reactivity due to the superior basicity of the surface O atoms when stretched. These results can be extended to the dissociation of other rather inert bonds like C–H, for which homolytic and heterolytic mechanisms can be also envisaged.

Overall, this work demonstrates that the use of computational methods is crucial for elucidating and shaping our current comprehension of reaction mechanisms. Furthermore, it proves that theory has unique capacities in the description of subtle concepts for which the indirect evidence provided by experiments cannot be conclusive. The knowledge acquired herein

may pave the way for the efficient use of CeO_2 in hydrogenation reactions and for the further advance in processes involving dissociation of non-polar bonds.

Supporting Information. Benchmark calculations with the HSE06 hybrid functional, electron localization in **I2**, statistics for linear fittings in Figure 4, electrostatic analysis for **I2'**, PDOS of CeO_2(111) surfaces, and details on the calculation of centers of the O(2p) band in the PDOS. This material is available free of charge via the Internet at http://pubs.acs.org.

Corresponding authors. E-mail: maxgarcia@iciq.es; nlopez@iciq.es; Fax: (+34)977 92 02 24; Tel: (+34)977 92 02 00.

Author contributions. The manuscript was written through contributions of all authors. All authors have given approval to the final version of the manuscript.

Notes. The authors declare no competing financial interests.

Acknowledgments. We thank EU (ERC-2010-StG-258406) and MINECO (CTQ2012-33826/BQU) for financial support and BSC-RES for generously providing access to their computational resources.

References

(1) Henrich, V. E.; Cox, P. A., *The Surface Science of Metal Oxides*; Cambridge University Press: Cambridge, U.K., 1994; Chapter 6, p. 247.

(2) Fierro, J. L. G., *Metal Oxides: Chemistry and Applications*; CRC Press: Boca Raton, FL, 2006.

(3) Gribov, E. N.; Bertarione, S.; Scarano, D.; Lamberti, C.; Spoto, G.; Zecchina, A. Vibrational and Thermodynamic Properties of H_2 Adsorbed on MgO in the 300-20 K Interval. *J. Phys. Chem. B*, **2004**, *108*, 16174–16186.

(4) Chen, H.-Y. T.; Giordano, L.; Pacchioni, G. From Heterolytic to Homolytic H_2 Dissociation on Nanostructured MgO(001) Films As a Function of the Metal Support. *J. Phys. Chem. C*, **2013**, *117*, 10623–10629.

(5) Joubert, J.; Salameh, A.; Krakoviack, V.; Delbecq, F.; Sautet, P.; Copéret, C.; Basset, J. M. Heterolytic Splitting of H_2 and CH_4 on γ-Alumina as a Structural Probe for Defect Sites. *J. Phys. Chem. B*, **2006**, *110*, 23944–23950.

(6) Binet, C.; Daturi, M.; Lavalley, J.-C. IR Study of Polycrystalline Ceria Properties in Oxidised and Reduced States. *Catal. Today*, **1999**, *50*, 207–225.

(7) Chen, H.-T.; Choi, Y. M.; Liu, M.; Lin, M. C. A Theoretical Study of Surface Reduction Mechanisms of CeO_2(111) and (110) by H_2. *ChemPhysChem*, **2007**, *8*, 849–855.

(8) Menetrey, M.; Markovits, A.; Minot, C. Reactivity of a Reduced Metal Oxide Surface: Hydrogen, Water and Carbon Monoxide Adsorption on Oxygen Defective Rutile TiO_2(110). *Surf. Sci.*, **2003**, *524*, 49–62.

(9) Deluga, G. A.; Salge, J. R.; Schmidt, L. D.; Verykios, X. E. Renewable Hydrogen from Ethanol by Autothermal Reforming. *Science*, **2004**, *303*, 993–997.

(10) Zhang, B.; Tang, X.; Li, Y.; Xu, Y.; Shen, W. Hydrogen Production from Steam Reforming of Ethanol and Glycerol over Ceria-supported Metal Catalysts. *Int. J. Hydrogen Energy*, **2007**, *32*, 2367–2373.

(11) Fu, Q.; Saltsburg, H.; Flytzani-Stephanopoulos, M. Active Nonmetallic Au and Pt Species on Ceria-based Water-Gas Shift Catalysts. *Science*, **2003**, *301*, 935–938.

(12) Rodríguez, J. A.; Hanson, J. C.; Stacchiola, D.; Senanayake, S. D. In Situ/Operando Studies for the Production of Hydrogen through the Water-Gas Shift on Metal Oxide Catalysts. *Phys. Chem. Chem. Phys.*, **2013**, *15*, 12004–12025.

(13) Vilé, G.; Bridier, B.; Wichert, J.; Pérez-Ramírez, J. Ceria in Hydrogenation Catalysis: High Selectivity in the Conversion of Alkynes to Olefins. *Angew. Chem. Int. Ed.*, **2012**, *51*, 8620–8623.

(14) Carrasco, J.; Vilé, G.; Fernández-Torre, D.; Pérez, R.; Pérez-Ramírez, J.; Ganduglia-Pirovano, M. V. Molecular-Level Understanding of CeO_2 as a Catalyst for Partial Alkyne Hydrogenation. *J. Phys. Chem. C*, **2014**, *118*, 5352–5360.

(15) Trovarelli, A. *Catalysis by Ceria and Related Materials*; Imperial College Press: London, U.K., 2002; p. 528.

(16) Murray, E. P.; Tsai, T.; Barnett, S. A. A Direct-Methane Fuel Cell with a Ceria-based Anode. *Nature*, **1999**, *400*, 649–651.

(17) McIntosh, S.; Gorte, R. J. Direct Hydrocarbon Solid Oxide Fuel Cells. *Chem. Rev.*, **2004**, *104*, 4845–4866.

(18) Amrute, A. P.; Mondelli, C.; Moser, M.; Novell-Leruth, G.; López, N.; Rosenthal, D.; Farra, R.; Schuster, M. E.; Teschner, D.; Schmidt, T. *et al*. Performance, Structure, and Mechanism of CeO_2 in HCl Oxidation to Cl_2. *J. Catal.*, **2012**, *286*, 287–297.

(19) Moser, M.; Mondelli, C.; Schmidt, T.; Girgsdies, F.; Schuster, M. E.; Farra, R.; Szentmiklósi, L.; Teschner, D.; Pérez-Ramírez, J. Supported CeO_2 Catalysts in Technical Form for Sustainable Chlorine Production. *Appl. Catal. B*, **2013**, *132–133*, 123–131.

(20) Paier, J.; Penschke, C.; Sauer, J. Oxygen Defects and Surface Chemistry of Ceria: Quantum Chemical Studies Compared to Experiment. *Chem. Rev.*, **2013**, *113*, 3949–3985.

(21) Laachir, A.; Perrichon, V.; Badri, A.; Lamotte, J.; Catherine, E.; Lavalley, J. C.; El Fallah, J.; Hilaire, L.; Le Normand, F.; Quéméré, E. *et al*. Reduction of CeO_2 by Hydrogen. Magnetic Susceptibility and Fourier-transform Infrared, Ultraviolet and X-ray

Photoelectron Spectroscopy Measurements. *J. Chem. Soc., Faraday Trans.*, **1991**, *87*, 1601–1609.

(22) Boaro, M.; Vicario, M.; de Leitenburg, C.; Dolcetti, G.; Trovarelli, A. The Use of Temperature-Programmed and Dynamic/Transient Methods in Catalysis: Characterization of Ceria-based, Model Three-Way Catalysts. *Catal. Today*, **2003**, *77*, 407–417.

(23) Désaunay, T.; Bonura, G.; Chiodo, V.; Freni, S.; Couzinié, J. P.; Bourgon, J.; Ringuedé, A.; Labat, F.; Adamo, C.; Cassir, M. Surface-Dependent Oxidation of H_2 on CeO_2 Surfaces. *J. Catal.*, **2013**, *297*, 193–201.

(24) Jacox, M. E. Vibrational and Electronic Energy Levels of Polyatomic Transient Molecules. Supplement B. *J. Phys. Chem. Ref. Data, Suppl. B*, **2003**, *32*, 1–441.

(25) Sohlberg, K.; Pantelides, S. T.; Pennycook, S. J. Interactions of Hydrogen with CeO_2. *J. Am. Chem. Soc.*, **2001**, *123*, 6609–6611.

(26) Vicario, G.; Balducci, G.; Fabris, S.; de Gironcoli, S.; Baroni, S. Interaction of Hydrogen with Cerium Oxide Surfaces: A Quantum Mechanical Computational Study. *J. Phys. Chem. B*, **2006**, *110*, 19380–19385.

(27) Watkins, M. B.; Foster, A. S.; Shluger, A. L. Hydrogen Cycle on CeO_2 (111) Surfaces: Density Functional Theory Calculations. *J. Phys. Chem. C*, **2007**, *111*, 15337–15341.

(28) Marrocchelli, D.; Yildiz, B. First-Principles Assessment of H_2S and H_2O Reaction Mechanisms and the Subsequent Hydrogen Absorption on the CeO_2(111) Surface. *J. Phys. Chem. C*, **2011**, *116*, 2411–2424.

(29) Alam, M. K.; Ahmed, F.; Miura, R.; Suzuki, A.; Tsuboi, H.; Hatakeyama, N.; Endou, A.; Takaba, H.; Kubo, M.; Miyamoto, A. Surface Reduction Processes of Cerium Oxide

Surfaces by H_2 using Ultra Accelerated Quantum Chemical Molecular Dynamic Study. *Catal. Today*, **2011**, *164*, 9–15.

(30) Kresse, G.; Furthmuller, J. Efficient Iterative Schemes for Ab Initio Total-Energy Calculations using a Plane-Wave Basis Set. *Phys. Rev. B*, **1996**, *54*, 11169–11186.

(31) Kresse, G.; Furthmuller, J. Efficiency of Ab-Initio Total Energy Calculations for Metals and Semiconductors using a Plane-Wave Basis Set. *Comput. Mater. Sci.*, **1996**, *6*, 15–50.

(32) Blöchl, P. E. Projector Augmented-Wave Method. *Phys. Rev. B*, **1994**, *50*, 17953–17979.

(33) Perdew, J. P.; Burke, K.; Ernzerhof, M. Generalized Gradient Approximation Made Simple. *Phys. Rev. Lett.*, **1996**, *77*, 3865–3868.

(34) Dudarev, S. L.; Botton, G. A.; Savrasov, S. Y.; Humphreys, C. J.; Sutton, A. P. Electron-Energy-Loss Spectra and the Structural Stability of Nickel Oxide: An LSDA+U Study. *Phys. Rev. B*, **1998**, *57*, 1505–1509.

(35) Ganduglia-Pirovano, M. V.; Da Silva, J. L. F.; Sauer, J. Density-Functional Calculations of the Structure of Near-Surface Oxygen Vacancies and Electron Localization on CeO_2(111). *Phys. Rev. Lett.*, **2009**, *102*, 026101–4.

(36) Fernández-Torre, D.; Kośmider, K.; Carrasco, J.; Ganduglia-Pirovano, M. V.; Pérez, R. Insight into the Adsorption of Water on the Clean CeO_2(111) Surface with van der Waals and Hybrid Density Functionals. *J. Phys. Chem. C*, **2012**, *116*, 13584–13593.

(37) Farra, R.; García-Melchor, M.; Eichelbaum, M.; Hashagen, M.; Frandsen, W.; Allan, J.; Girgsdies, F.; Szentmiklósi, L.; López, N.; Teschner, D. Promoted Ceria: A Structural, Catalytic, and Computational Study. *ACS Catal.*, **2013**, *3*, 2256–2268.

(38) Kümmerle, E. A.; Heger, G. The Structures of C–$Ce_2O_{3+\delta}$, Ce_7O_{12}, and $Ce_{11}O_{20}$. *J. Solid State Chem.*, **1999**, *147*, 485–500.

(39) Da Silva, J. L. F.; Ganduglia-Pirovano, M. V.; Sauer, J.; Bayer, V.; Kresse, G. Hybrid Functionals Applied to Rare-Earth Oxides: The Example of Ceria. *Phys. Rev. B*, **2007**, *75*, 045121–10.

(40) Henkelman, G.; Arnaldsson, A.; Jónsson, H. A Fast and Robust Algorithm for Bader Decomposition of Charge Density. *Comput. Mater. Sci.*, **2006**, *36*, 354–360.

(41) Sanville, E.; Kenny, S. D.; Smith, R.; Henkelman, G. Improved Grid-based Algorithm for Bader Charge Allocation. *J. Comput. Chem.*, **2007**, *28*, 899–908.

(42) Tang, W.; Sanville, E.; Henkelman, G. A Grid-based Bader Analysis Algorithm without Lattice Bias. *J. Phys.: Condens. Matter*, **2009**, *21*, 084204–11.

(43) Henkelman, G.; Uberuaga, B. P.; Jónsson, H. A Climbing Image Nudged Elastic Band Method for Finding Saddle Points and Minimum Energy Paths. *J. Chem. Phys.* **2000**, *113*, 9901–9904.

(44) Krukau, A. V.; Vydrov, O. A.; Izmaylov, A. F.; Scuseria, G. E. Influence of the Exchange Screening Parameter on the Performance of Screened Hybrid Functionals. *J. Chem. Phys.*, **2006**, *125*, 224106–5.

(45) For **I2,** several open-shell singlet and triplet spin states with different localizations of the Ce^{+3} ions were calculated and found to have similar energies (energy differences ≤0.07 eV). These results are presented in Table S2.

(46) This energy barrier is in line with the value of 1.00 eV reported in Ref. 14, but significantly different from the 0.22 eV provided in Ref. 7.

(47) To assess possible structure sensitivity issues, the heterolytic product **I2'** was also located for the less stable CeO_2(110) surface. Similarly to the (111) surface, this species is also a

reaction minimum that displays a relatively short H–H distance, *i.e.* 1.741 Å, and an elongated O–H bond, *i.e.* 0.994 Å.

(48) Wischert, R.; Laurent, P.; Copéret, C.; Delbecq, F.; Sautet, P. *γ*-Alumina: The Essential and Unexpected Role of Water for the Structure, Stability, and Reactivity of "Defect" Sites. *J. Am. Chem. Soc.*, **2012**, *134*, 14430–14449.

(49) Wiberg, N. *Holleman-Wiberg's Inorganic Chemistry*; Academic Press: London, U.K., 2001; p. 1924.

(50) Metiu, H.; Chrétien, S.; Hu, Z.; Li, B.; Sun, X. Chemistry of Lewis Acid–Base Pairs on Oxide Surfaces. *J. Phys. Chem. C*, **2012**, *116*, 10439–10450.

(51) López, N.; Vitiello, M.; Illas, F.; Pacchioni, G. Interaction of H_2 with Strained Rings at the Silica Surface from Ab Initio Calculations. *J. Non-Cryst. Solids*, **2000**, *271*, 56–63.

(52) Zhu, H.-Z.; Lu, Y.-M.; Fan, F.-J.; Yu, S.-H. Selective Hydrogenation of Nitroaromatics by Ceria Nanorods. *Nanoscale*, **2013**, *5*, 7219–7223.

(53) Amakawa, K.; Sun, L.; Guo, C.; Hävecker, M.; Kube, P.; Wachs, I. E.; Lwin, S.; Frenkel, A. I.; Patlolla, A.; Hermann, K. *et al*. How Strain Affects the Reactivity of Surface Metal Oxide Catalysts. *Angew. Chem. Int. Ed.*, **2013**, *52*, 13553–13557.

(54) Akhade, S. A.; Kitchin, J. R. Effects of Strain, *d*-band Filling, and Oxidation State on the Surface Electronic Structure and Reactivity of *3d* Perovskite Surfaces. *J. Chem. Phys.*, **2012**, *137*, 084703–9.

(55) McFarland, E. W.; Metiu, H. Catalysis by Doped Oxides. *Chem. Rev.*, **2013**, *113*, 4391–4427.

Table of Contents (TOC) image